Predicting Model for Tumor Budding Status using Radiomics Features of 18F-PET/CT and in Cervical Cancer

Gun Oh Chong
Kyungpook National University School of Medicine
Shin-Hyung Park
Kyungpook National University School of Medicine
Shin Young Jeong (syjeong@knu.ac.kr)
Kyungpook National University School of Medicine/Hospital
Su Jeong Kim
Kyungpook National University School of Medicine
Jee Young Park
Kyungpook National University School of Medicine
Yoon Hee Lee
Kyungpook National University School of Medicine
Sang-Woo Lee
Kyungpook National University School of Medicine
Dae Gy Hong
Kyungpook National University School of Medicine
Ji Young Park
Kyungpook National University School of Medicine
Hyung Soo Han
Kyungpook National University School of Medicine

Research Article

Keywords: Cervical cancer, tumor budding, radiomics, 18F-FDG PET/CT, predicting model

Posted Date: March 12th, 2021

DOI: https://doi.org/10.21203/rs.3.rs-280398/v1

Abstract

Objective

The aim of this study was to compare radiomics feature on ^{18}F-FDG PET/CT and intratumoral heterogeneity according to tumor budding (TB) status and to develop predicting model for TB status using radiomics feature of ^{18}F-FDG PET/CT in patients with cervical cancer.

Materials and methods

A total of 76 cervical cancer patients who performed radical hysterectomy and preoperative ^{18}F-FDG PET/CT were included. We assessed the status of intratumoral budding (ITP) and peritumoral budding (PTB) in all available hematoxylin and eosin-stained specimens. Three conventional metabolic parameters and a total of 59 features were extracted and analyzed. Univariate analysis was used to identify significant metabolic parameters and radiomics findings for TB status. Predicting model for TB status was built by the LASSO regularization.

Results

The univariate analysis lead to the identification of 2 significant metabolic parameters and 12 significant radiomic features according to ITB status. Among these parameters, only compacity was remained in multivariate analysis for ITB status (odds ratio. 5.0047; 95% confidence interval, 1.1636 – 21.5253; p = 0.0305). Five radiomics features (Kurtosis, Compacity, Short-Zone Low Gray-level Emphasis, Coarseness, Low Gray-level Run Emphasis) were selected by the LASSO regularization and the predicting model for ITB status had a mean area under curve of 0.810 in training dataset and 0.794 in validation dataset.

Conclusion

Radiomics features on ^{18}F-FDG PET/CT was associated with ITB status. The predicting model using radiomics features successfully predicted TB status in cervical cancer. The predicting models for ITB status may contribute to personalized medicine in the management of cervical cancer patients.

Introduction

Tumor budding (TB) is defined as a single neoplastic cell or cell cluster of up to four neoplastic cells at the invasive front of the tumor (peritumoral budding, PTB) or within the tumor mass (intratumoral budding, ITB) [1]. Several studies have demonstrated that TB was associated with lymphovascular invasion (LVI), lymph node metastasis, disease recurrence, and an unfavorable survival outcome, especially in colorectal cancer [2], esophageal carcinoma [3], and head and neck cancer [4]. Recently we evaluated prognostic roles of TB and correlation between TB and conventional pathologic parameters in gynecological cancers [5,6]. TB was associated with deep depth invasion, higher International Federation of Gynecologic Obstetrics (FIGO) stage, LVI, and lymph node metastasis in endometrial cancer [5].

Moreover, high TB was an independent prognostic factor for predicting survival outcomes in cervical cancer [6].

Currently, F-18 fluorodeoxyglucose positron emission tomography/computed tomography (^{18}F-FDG PET/CT) has been widely used to detect lymph node involvement, distant metastasis, and recurrent disease in cervical cancer [7]. Various metabolic parameters of ^{18}F-FDG PET/CT have been reported as prognostic factors including maximum standardized uptake value (SUVmax), metabolic tumor volume (MTV), and total lesion glycolysis (TLG). Radiomics studies, which represent intratumoral heterogeneity have emerged as a new and exciting study area in recent years. The measurement of texture indices from tumor ^{18}F-FDG PET/CT images has been recently proposed as an adjunct to predict tumor response to therapy. There is emerging evidence that intratumoral metabolic heterogeneity on pre-treatment ^{18}F-FDG PET/CT might be a predictor of tumor recurrence after treatment in patients with lung cancer, esophageal cancer, head and neck cancer, and cervical cancer [8-11]. Furthermore, recent studies showed ^{18}F-FDG PET/CT radiomics using various textural features were potential biomarker to predict tumor recurrence and lymph node metastasis [12-13]. Tumor heterogeneity is defined by the presence of different cell subpopulations or clones and has a fundamental role in growth, progression, and therapeutic resistance. Tumor hypoxia, angiogenesis, necrosis, fibrosis, cell proliferation, and inflammation process play a role in tumor heterogeneity [14]. Epithelial-mesenchymal transition (EMT) of primary tumor tissues may lead loss of cell-to-cell adhesion and individual cells or small groups of cells acquired the ability to migrate and invade through the surrounding tissues. Moreover, TB may lead to a more aggressive clinicopathologic characteristics through similar mechanism of EMT such as increased extracellular matrix degradation, increased migration, and loss of cell adhesion [15]. These EMT processes are accompanied by changes in cell morphology [16] and may lead to change tumor heterogeneity. However, there has been no study which evaluate correlation between metabolic parameters and radiomics finding of ^{18}F- FDG PET/CT and TB in cervical cancer. So, we hypothesized TB may associate with higher metabolic parameters in ^{18}F-FDG PET/CT because of aggressive behavior of TB and radiomics finding may different according to TB status because TB is individual cells and small groups of cells.

The aim of this study was to compare radiomics feature on ^{18}F-FDG PET/CT and intratumoral heterogeneity according to TB status and to develop predicting model for TB status using radiomics feature of ^{18}F-FDG PET/CT in patients with cervical cancer.

Materials And Methods

Patients

After approval of the Institutional Review Board of Kyungpook National University Chilgok Hospital (KNUCH 2020-03-011), we reviewed the archival medical records and hematoxylin and eosin (H&E)-stained slides of early-stage and locally advanced cervical cancer patients. The need for informed consent was waived because of the retrospective nature of the study. A total of 136 patients who

underwent radical hysterectomy with pelvic and/or paraaortic lymphadenectomy for the treatment of early-stage and locally advanced cervical cancer were included. Among the 136 patients, 76 patients performed preoperative ^{18}F-FDG PET/CT and were enrolled in this study. The enrolled patients were semi-randomly divided into a training dataset (51 patients) and a test set (25 patients) by using the “doBy” R package while preserving the distribution of ITB status. Patients with a history of preoperative chemotherapy, radiotherapy, or synchronous malignancies were excluded. The patients were clinically staged according to the 2009 International Federation of Gynecologic Obstetrics (FIGO) staging system [17].

Histopathological evaluation

Specimens were examined from multiple sections of the whole tumor areas and were stained with hematoxylin and eosin (H&E). For each case, all available specimens were independently reviewed for the detailed histopathological features and the quantitative assessment of TB by two pathologists (J.Y.P and J.Y.P) in a blinded manner without information about the clinicopathological data and outcomes.

The pathological parameters included tumor size, FIGO stage, histological subtype, deep stromal invasion, LVI, parametrial invasion, lymph node metastasis, and the number and distribution of TB. TB was defined as an isolated single cancer cell or small cell clusters composed of 4 tumor cells or less located at the advancing edge (PTB) and within the tumor area (ITB).

^{18}F-FDG PET/CT Image Acquisition

All patients fasted for at least six hours, and their blood glucose levels were determined before the administration of ^{18}F-FDG. Patients with blood glucose levels higher than 150 mg/dL were rescheduled for a later examination, and treatment was administered to maintain a blood glucose concentration of less than 150 mg/dL in all participants. Patients received intravenous injections of approximately 5.2 MBq of FDG per kilogram of body weight and were advised to rest for one hour before undergoing the acquisition of ^{18}F-FDG PET/CT images. The ^{18}F-FDG PET/CT scans were performed using Discovery 600 (GE Healthcare, Chicago, IL, USA). Before the PET scan, for attenuation correction, a low-dose CT scan was obtained without contrast enhancement from the skull base to the thigh while the patient was in the supine position and breathing quietly. PET scans were also obtained from the skull base to the thigh at 2.5 min per bed position. PET images were reconstructed with a 128 X 128 matrix and an ordered-subset expectation maximum iterative reconstruction algorithm.

Image Interpretation and PET Image Analyses

The ^{18}F-FDG PET/CT images were interpreted by two experienced nuclear medicine physicians, and a final consensus was achieved for all patients. A positive finding was defined as any focus with increased FDG uptake as compared with the surrounding normal tissue. Foci of FDG uptake due to normal physiology or benign variants, such as muscular exercise or an infectious pulmonary infiltration, were excluded from the analysis.

All image analyses were performed using the Advantage Workstation 4.5 software (GE Medical Systems, Waukesha, WI, USA). The primary tumor lesion was delineated by the volume of interest using an isocontour threshold method based on the SUV, and metabolic PET parameters were assessed. SUVmax values were based on body weight and were calculated using the following formula: SUVmax = maximum activity in the region of interest (MBq/g)/[injected dose (MBq) ÷ bodyweight (g)]. SUVmax was designated as the highest value of SUVmax of the primary tumor. The MTV was determined as the volume of voxels with a threshold SUV of the mediastinal blood pool, because the mediastinal blood pool has been regarded as the preferred site for measuring background activity [18]. The mean SUV of the mediastinal SUV values was determined by drawing a region of interest over contiguous slices on descending aorta carefully excluding the walls from the region of interest. The mean SUV of the mediastinal background plus 2 SDs was used as the threshold to automatically calculate MTV [17]. The TLG was calculated as the MTV multiplied by the SUVmean of the lesion. The MTV and TLG were also obtained for the primary tumor.

Statistical analysis

The differences between subsets were evaluated with a Student's t-test or Mann-Whitney test, and differences between proportions were compared with the chi square test or Fisher's exact test. To identify an optimal cutoff value of metabolic parameters and radiomics finding of ^{18}F-PET/CT for the prediction of ITB status, ROC curve analysis was performed. Multiple logistic regression analysis was used to evaluate metabolic parameters and radiomics finding of ^{18}F-PET/CT for ITB status. Estimated odds ratios (ORs) with 95% confidence intervals (95% CIs) were presented. All statistical tests were 2-sided, and a *p*-value of <0.05 was considered significant. Statistical analysis was performed using SPSS software version 22.0 (SPSS, Chicago, IL, USA) and Medcalc version 15.4 (Medcalc Software, Ostend, Belgium), and R version 3.6.3 (R foundation for Statistical Computing, Vienna, Austria). The R packages "caret", "glmnet", "MASS", and "pROC" were used for analysis.

Radiomics analysis

Radiomics features were extracted using the LIFEx package (http://www.lifexsoft.org) [19]. LifeX was set up using the following input parameters for calculation of features: 64 Gy levels to resample the ROI content which was performed in absolute terms between a minimum of 0 and a maximum of 20 [20]. A total of 59 features were extracted from the analysis of the volumes inspected. These indices included conventional parameters, shape and size features, histogram-based features, second and high order-based features. The correction for the partial volume effect was not applied. In the analysis were included all primary tumor lesions, irrespectively of their volume but LifeX calculates the shape and size indices as well as second order (gray-level co-occurrence matrix [GLCM]) and high order-based (neighborhood gray-level different matrix [NGLDM], gray-level run length matrix, [GLRLM] and gray-level zone-length matrix [GLZLM]) features only for ROI of at least 64 voxels due to technical reasons. The features calculated are summarized in supplementary Table 1.

Each feature value was normalized using z-score normalization (z = (x − mean(x))/SD(x)) (standard deviation [SD])). Feature selection process consisted of two steps in the training dataset. First, t-test was performed to screen potential features throughout radiomics features and conventional metabolic parameters. Only features with $p < 0.05$ were considered significant and entered further selection step. Next, the least absolute shrinkage and selection operator (LASSO) regression was used to select key features to build prediction model, with a 3-fold cross validation.

After feature selection process, the prediction models were constructed using a random forest (RF), a support vector machine (SVM), and a neural network (NN) using training dataset. The constructed model performance was validated independently in the test dataset by the area under the receiver operating characteristic (ROC) curve. The R packages “randomForest”, “kernlab”, and “neuralnet” were used for building prediction model.

Results

Clinicopathologic features and treatment outcomes

The clinicopathologic characteristics of the study participants are listed in Table 1. The predominant FIGO stage was IB1 (n = 43 [56.6%]), followed by IB2 (n = 14 [18.4%]), IIB (n = 10 [13.2%]), and IIA (n = 9 [11.8%]). The histologic cervical cancer types were as follows: squamous cell carcinoma (n = 91 [66.9%]), adenocarcinoma (n = 37 [27.2%]), and adenosquamous carcinoma (n = 8 [5.9%], Table 1). The median ITB counts (range) were 3.5 (0-40), and the median PTB counts (range) were 4 (0-44), respectively. ITB was observed in 47 patients (61.8%), and PTB in 62 patients (81.6%), respectively.

Comparison of metabolic parameters and radiomics features of ^{18}F-PET/CT according to TB status

The median SUVmax significantly higher in positive ITB group than in negative ITB group (11.35 vs. 8.37, $p = 0.0406$; Figure 1). However, the median SUVmax was not different according to the PTB status. Among the radiomics features, EntropyGLCM (GLCM, $p = 0.0111$), Coarseness (NGLDM, $p = 0.0497$), Low Gray-level Run Emphasis / Long-Run Low Gray-level Emphasis (GLRLM, $p = 0.0189$ and $p = 0.0101$, respectively), Low Gray-level Zone Emphasis / Short-Zone Low Gray-level Emphasis / Zone Length Non-Uniformity Zone (GLZLM, $p = 0.0137$, $p = 0.0154$, and $p = 0.0056$, respectively), Sphericity / Compacity (Shape and Size, $p = 0.0065$ and $p = 0.0108$, respectively), and Kurtosis / $\text{Entropy}_{\text{Hist}}$ / $\text{Energy}_{\text{Hist}}$ (Histogram, $p = 0.0267$, $p = 0.0130$, and $p = 0.0200$) had significant different levels according to the ITB status. However, there was no significant different radiomics findings according to the PTB status (Table 2).

Multiple logistic regression analysis for ITB status

Univariate and multivariate analysis were performed for evaluation of correlation between ^{18}F-FDG PET/CT values and ITB status using multiple logistic regression analysis (Table 3). Among the significant parameters of conventional metabolic parameters (SUVmax, MTV, and TLG) and each radiomics findings

(GLCM, NGLDM, GLZLM, Shape and Size, and Histogram) in univariate analysis, the most significant parameters (the lowest *p* value) were included to multivariate analysis for inhibition of conflicting each parameters. In univariate analysis, SUVmax (OR, 3.34; 95% CI, 1.27-8.79; $p = 0.0146$), TLG (OR, 4.42% CI, 1.33-14.72; $p = 0.0154$), EntropyGLCM (OR, 5.36; 95% CI, 1.95-14.69; $p = 0.0011$), Coarseness (OR, 3.94; 95% CI, 1.41-11.03; $p = 0.0090$), Low Gray-level Run Emphasis (OR, 3.45; 95% CI, 1.26-9.47; $p = 0.0161$), Long-Run Low Gray-level Emphasis (OR, 3.34; 95% CI, 1.27-8.79; $p = 0.0146$), Low Gray-level Zone Emphasis (OR, 4.05; 95% CI, 1.52-10.82; $p = 0.0052$) Short-Zone Low Gray-level Emphasis (OR, 3.94; 95% CI, 1.41-11.03; $p = 0.0090$), Zone Length Non-Uniformity Zone (OR, 9.16; 95% CI, 1.27-8.79; $p = 0.0146$), Sphericity (OR, 6.09; 95% CI, 2.15-17.28; $p = 0.0007$), Compacity (OR, 8.73; 95% CI, 2.48-30.76; $p = 0.0007$), Kurtosis (OR, 3.96; 95% CI, 1.38-11.38; $p = 0.0106$), $\text{Entropy}_{\text{Hist}}$ (OR, 5.98; 95% CI, 2.12-16.86; $p = 0.0007$), and $\text{Energy}_{\text{Hist}}$ (OR, 5.98; 95% CI, 2.12-16.86; $p = 0.0007$) were significant parameters which correlated with positive ITB. Multivariate analysis with the enter methods showed only Compacity (OR, 5.00; 95% CI, 1.16-21.53; $p = 0.0305$) remained independent parameter correlated with positive ITB (Table 3).

Predicting model for ITB status usingradiomics features of ^{18}F-FDG PET/CT

A total of 48 features were significant parameters in t-test and were subjected to further selection step by the LASSO regularization (Figure 1). Among them, the final 27 remaining features (SUVmax, MTV, SUV_Skewness, discretized_SUVmax, discretized_SUV_Skewness, discretized_SUV_Kurtosis, discretized_SUVpeak_Sphere, discretized_HISTO_ExcessKurtosis, GLCM_Entropy_log2, GLCM_Dissimilarity, GLRLM_LRE, GLRLM_LGRE, GLRLM_SRHGE, GLRLM_LRLGE, GLRLM_GLNU, GLRLM_RLNU, NGLDM_Contrast, NGLDM_Busyness, GLZLM_SZE, GLZLM_LZE0, GLZLM_LGZE, GLZLM_HGZE, GLZLM_SZLGE, GLZLM_SZHGE, GLZLM_LZLGE) were selected. Figure 2 shows the ROC curves of the prediction models by three machine learning algorithms in training and test dataset. The AUC values of the prediction models constructed by the RF, SVM, and NN were 1.000, 0.951, and 1.000, respectively, in the training dataset and 0.752, 0.784, 0.752, respectively, in the test dataset.

Discussion

In this study, radiomics features of ^{18}F-FDG PET/CT was associated with TB status especially in ITB status. Among the 59 features, 12 features were significantly different according to the ITB status in univariate logistic regression analysis. Among these 12 features, compacity was the most significant parameter for ITB status in multivariate logistic regression analysis. Moreover, we developed the predicting model for ITB status using 5 features by the LASSO regularization, and AUC was 0.810.

Radiomics is relatively new and evolving field in medical imaging in which many features are extracted from medical images analysis and interpretation using bioinformatic approaches [14]. Furthermore, radiomics precision medicine and tumor heterogeneity have become one of the hottest topics in the oncological medical area in recent years [21]. At the biological level, it has been recognized that heterogeneity of tumor microenvironment might be reflected in medical images, with respect to cellular density, proliferation, angiogenesis, hypoxia, receptor expression, necrosis, fibrosis, and inflammation and

these factors might contribute to a more aggressive phenotype and poor treatment responses [22]. Therefore, radiomics signature might represent segmentation of tumor subregions with different biological characteristics and contribute to treatment response and prognosis.

In colorectal cancer, high ITB correlated with higher tumor grade, higher pT stage, lymphatic invasion, vascular invasion, nodal metastasis, and shorter survival time [23]. ITB may lead to a more aggressive clinicopathologic characteristics through similar mechanism for PTB such as increased extracellular matrix degradation, increased migration, and loss of cell adhesion [15]. So, we hypothesized ITB may associate with higher metabolic parameters because of aggressive behavior of ITB. Moreover, radiomics finding may different according to ITB status because TB is individual cells and small groups of cells owing to loss of cell adhesion.

To date only one study recently demonstrated correlation between tumor cancer cell metabolism and morphologic features of aggressiveness as assessed by microscopy such as TB [24]. MTV was higher in TB group than in non-TB group with marginal significant (p = 0.06) in laryngeal and pharyngeal carcinoma [25]. In this study, SUVmax was significantly different according to ITB status (p = 0.0406). Moreover, SUVmax and TLG were associated with ITB status in univariate logistic regression analysis (p = 0.0146 and p = 0.0154, respectively). More aggressive nature of ITB may represent higher metabolic parameters in ^{18}F-FDG PET/CT.

EMT of primary tumor tissues may lead loss of cell-to-cell adhesion and occurrence ITB. So, ITB may lead segmentation of tumor subregions with different biological characteristics and these may contribute tumor heterogeneity. However, no study has been reported about correlation between ITB and radiomics findings. In this study, 12 features were associated with ITB status and compacity was powerful biomarker which represent ITB status in multivariate logistic regression analysis. Previous study demonstrated that among the radiomics features, the most significant covariate was compacity for predict local control and survival in hepatocellular carcinoma [26].

Previous our study showed that tumors with high TB were significantly associated with LVI, deep stromal invasion, parametrial invasion and lymph node metastasis in cervical cancer [6]. Preoperative prediction of TB status may helpful to personalized medicine such as decision of radicality of surgery or extent of lymphadenectomy. However, TB status was finally determined by postoperative surgical specimens. To date, there was no modality with estimate TB status preoperatively. Therefore, predicting models were constructed for ITB status using both conventional metabolic parameters and radiomics features from ^{18}F-FDG PET/CT scans. Among the 48 features which were significant parameters in univariate logistic regression, 27 features were selected by the t-test and LASSO regularization. The AUC values of the prediction models were greater than 0.75 in the test dataset.

The main limitations of this study are its retrospective nature and small sample size, which may have contributed to selection bias. In addition, it is a single-center study; therefore, the generalization of our findings are limited. Despite these limitations, our study offers some unique and significant findings. Our

study showed correlations between radiomics findings and TB status for the first time. Moreover, we established the predicting models for ITB status using radiomics feature in ^{18}F-FDG PET/CT.

In conclusion, higher metabolic quantities were observed in positive ITB group than in negative ITB group. Radiomics findings in ^{18}F-FDG PET/CT was associated with ITB status, and among these features, the most significant covariate was compacity for ITB status. Furthermore, prediction models for ITB status using radiomics findings in ^{18}F-FDG PET/CT may contribute to personalized medicine in cervical cancer.

Declarations

Fungding

This work was supported by the National Research Foundation of Korea (NRF) grant funded by the Korea government (MIST) (No. 2020R1G1A1102848). This work was supported by a grant from the Korea Health Technology R&D Project through the Korea Health Industry Development Institute (KHIDI), funded by the Ministry of Health &Welfare, Republic of Korea (Grant Number: HI16C1501).

Conflicts of interest

The authors declare that they have no conflict of interest.

Ethics approval

This study is approved by Institutional Review Board (IRB) of Kyungpook National University Chilgok Hospital (IRB no. KNUCH 2020-03-011)

Informed consent

Informed consent was waived, owing to the retrospective nature of the study.

Author contributions

Conceptualization: [Gun Oh Chong], [Shin Young Jeong], [Shin-Hyung Park], [Ji Young Park], [Hyung Soo Han]

Methodology: [Gun Oh Chong], [Su Jeong Kim], [Yoon Hee Lee], [Jee Young Park], [Ji Young Park], [Shin Young Jeong], [Sang-Woo Lee]

Formal analysis and investigation: [Gun Oh Chong], [Shin-Hyung Park], [Shin Young Jeong], [Yoon Hee Lee], [Sang-Woo Lee], [Dae Gy Hong]

Writing - original draft preparation: [Gun Oh Chong], [Shin-Hyung Park], [Jee Young Park], [Shin Young Jeong], [Su Jeong Kim]

Writing - review and editing: [Yoon Hee Lee], [Jee Young Park], [Ji Young Park], [Sang-Woo Lee], [Dae Gy Hong], [Hyung Soo Han]

Funding acquisition: [Gun Oh Chong], [Sang-Woo Lee], [Hyung Soo Han]

Resources: [Gun Oh Chong], [Shin Young Jeong], [Shin-Hyung Park], [Su Jeong Kim], [Jee Young Park], [Yoon Hee Lee], [Hyung Soo Han]

Supervision: [Sang-Woo Lee], [Dae Gy Hong], [Ji Young Park], [Hyung Soo Han]

References

1. Lugli A, Kirsch R, Ajioka Y, Bosman F, Cathomas G, Dawson H, et al. Recommendations for reporting tumor budding in colorectal cancer based on the International Tumor Budding Consensus Conference (ITBCC) 2016. Mod Pathol. 2017;30(9):1299-1311. doi: 10.1038/modpathol.2017.46. Epub 2017 May 26. Review.
2. Graham RP, Vierkant RA, Tillmans LS, Wang AH, Laird PW, Weisenberger DJ, et al. Tumor Budding in Colorectal Carcinoma: Confirmation of Prognostic Significance and Histologic Cutoff in a Population-based Cohort. Am J Surg Pathol. 2015;39(10):1340-6. doi: 10.1097/PAS.0000000000000504.
3. Almangush A, Karhunen M, Hautaniemi S, Salo T, Leivo I. Prognostic value of tumour budding in oesophageal cancer: a meta-analysis. Histopathology. 2016;68(2):173-82. doi: 10.1111/his.12781. Epub 2015 Sep 3. Review.
4. Almangush A, Salo T, Hagström J, Leivo I. Tumour budding in head and neck squamous cell carcinoma - a systematic review. Histopathology. 2014;65(5):587-94. doi: 10.1111/his.12471. Epub 2014 Oct 6. Review.
5. Park JY, Hong DG, Chong GO, Park JY. Tumor Budding is a Valuable Diagnostic Parameter in Prediction of Disease Progression of Endometrial Endometrioid Carcinoma. Pathol Oncol Res. 2019;25(2):723-730. doi: 10.1007/s12253-018-0554-x. Epub 2019 Jan 2.
6. Park JY, Chong GO, Park JY, Chung D, Lee YH, Lee HJ, et al. Tumor budding in cervical cancer as a prognostic factor and its possible role as an additional intermediate-risk factor. Gynecol Oncol. 2020;159(1):157-163. doi: 10.1016/j.ygyno.2020.07.030.
7. Wong TZ, Jones EL, Coleman RE. Positron emission tomography with 2-deoxy-2-[(18)F]fluoro-D-glucose for evaluating local and distant disease in patients with cervical cancer. Mol Imaging Biol. 2004;6(1):55-62.
8. Kim DH, Jung JH, Son SH, Kim CY, Hong CM, Oh JR, et al. Prognostic Significance of Intratumoral Metabolic Heterogeneity on 18F-FDG PET/CT in Pathological N0 Non-Small Cell Lung Cancer. Eur J Nucl Med Mol Imaging. 2014;41(11):2051-7.
9. Tixier F, Le Rest CC, Hatt M, Albarghach N, Pradier O, Metges JP, et al. tumor heterogeneity characterized by textural features on baseline 18F-FDG PET images predicts response to

concomitant radiochemotherapy in esophageal cancer. J Nucl Med. 2011;52(3):369-78.

10. Cheng NM, Fang YH, Chang JT, Huang CG, Tsan DL, Ng SH, et al. Textural features of pretreatment 18F-FDG PET/CT images: prognostic significance in patients with advanced T-stage oropharyngeal squamous cell carcinoma. J Nucl Med. 2013;54(10):1703-9.
11. Chong GO, Lee WK, Jeong SY, Park SH, Lee YH, Lee SW, et al. Prognostic value of intratumoral metabolic heterogeneity on F-18 fluorodeoxyglucose positron emission tomography/computed tomography in locally advanced cervical cancer patients treated with concurrent chemoradiotherapy. Oncotarget. 2017;28;8(52):90402-90412. doi: 10.18632/oncotarget.18769. eCollection 2017 Oct 27.
12. Reuzé S, Orlhac F, Chargari C, Nioche C, Limkin E, Riet F, et al. Prediction of cervical cancer recurrence using textural features extracted from 18F-FDG PET images acquired with different scanners. Oncotarget 2017 Jun 27;8(26):43169-43179. doi: 10.18632/oncotarget.17856.
13. Li XR, Jin JJ, Yu Y, Wang XH, Guo Y, Sun HZ. PET-CT radiomics by integrating primary tumor and peritumoral areas predicts E-cadherin expression and correlates with pelvic lymph node metastasis in early-stage cervical cancer. Eur Radiol. 2021 Feb 2. doi: 10.1007/s00330-021-07690-7.
14. Cook GJR, Azad G, Owczarczyk K, Siddique M, Goh V. Challenges and Promises of PET Radiomics. Eur J Nucl Med Mol Imaging. 2013;40(1):133-40. doi: 10.1007/s00259-012-2247-0. Epub 2012 Oct 13.
15. Zlobec I, Lugli A. Epithelial mesenchymal transition and tumor budding in aggressive colorectal cancer: tumor budding as oncotarget. Oncotarget. 2010;1(7):651-61.
16. Thiery JP, Sleeman JP. Complex networks orchestrate epithelial-mesenchymal transitions. Nat Rev Mol Cell Biol. 2006;7(2):131-42. doi: 10.1038/nrm1835.
17. Pecorelli S. Revised FIGO staging for carcinoma of the vulva, cervix, and endometrium. Int J Gynaecol Obstet. 2009;105:103-4.
18. Ziai P, Hayeri MR, Salei A, Salavati A, Houshmand S, Alavi A, et al. Role of Optimal Quantification of FDG PET Imaging in the Clinical Practice of Radiology. Radiographics. 2016;36(2):481-96. doi: 10.1148/rg.2016150102.
19. Wahl RL, Jacene H, Kasamon Y, Lodge MA. From RECIST to PERCIST: Evolving Considerations for PET response criteria in solid tumors. J Nucl Med. 2009;50 Suppl 1(Suppl 1):122S-50S. doi: 10.2967/jnumed.108.057307.
20. Nioche C, Orlhac F, Boughdad S, Reuzé S, Goya-Outi J, Robert C, et al. LIFEx: A Freeware for Radiomic Feature Calculation in Multimodality Imaging to Accelerate Advances in the Characterization of Tumor Heterogeneity. Cancer Res. 2018;15;78(16):4786-4789. doi: 10.1158/0008-5472.CAN-18-0125.
21. Valdora F, Houssami N, Rossi F, Calabrese M, Tagliafico AS. Rapid review: radiomics and breast cancer. Breast Cancer Res Treat. 2018 Jun;169(2):217-229. doi: 10.1007/s10549-018-4675-4.
22. Junttila MR, de Sauvage FJ. Influence of tumour micro-environment heterogeneity on therapeutic response. Nature. 2013 Sep 19;501(7467):346-54. doi: 10.1038/nature12626.
23. Lugli A, Vlajnic T, Giger O, Karamitopoulou E, Patsouris ES, Peros G, et al. Intratumoral budding as a potential parameter of tumor progression in mismatch repair-proficient and mismatch repair-deficient

colorectal cancer patients. Hum Pathol. 2011 Dec;42(12):1833-40. doi: 10.1016/j.humpath.2011.02.010.

24. Karpathiou G, Gavid M, Prevot-Bitot N, Dhomps A, Dumollard JM, Vieville M, et al. Correlation Between Semiquantitative Metabolic Parameters After PET/CT and Histologic Prognostic Factors in Laryngeal and Pharyngeal Carcinoma. Head Neck Pathol. 2020 Sep;14(3):724-732. doi: 10.1007/s12105-019-01116-z.
25. Cozzi L, Dinapoli N, Fogliata A, Hsu WC, Reggiori G, Lobefalo F, et al. Radiomics based analysis to predict local control and survival in hepatocellular carcinoma patients treated with volumetric modulated arc therapy. BMC Cancer. 2017 Dec 6;17(1):829. doi: 10.1186/s12885-017-3847-7.

Tables

Table 1. Clinicopathological and tumor budding characteristics.

Variables	
Age (years)	
Mean ± SD	47.95 ± 10.73
Median (range)	49 (25-74)
FIGO stage (n, %)	
IB1	43, 56.6
IB2	14, 18.4
IIA	9, 11.9
IIB	10, 13.2
Histology (n, %)	
Squamous cell carcinoma	54, 71.1
Adenocarcinoma/adenosquamous carcinoma	22, 28.9
Tumor size (cm)	
Mean ± SD	3.01 ± 1.67
Median (range)	3 (0-8.5)
Lymphovascular invasion (n, %)	59, 77.6
Deep stromal invasion (n, %)	46, 60.5
Parametrial invasion (n, %)	28, 36.8
Lymph node metastasis (n, %)	22, 28.9
Tumor budding characteristics	
Intratumor budding counts	
Mean ± SD	6.40 ± 9.61
Median (range)	3.5 (0-40)
Peritumoral budding counts	
Mean ± SD	7.49 ± 9.42
Median (range)	4 (0-44)
Intratumoral budding (n, %)	47, 61.8
Peritumoral budding (n, %)	62, 81.6

FIGO = International Federation of Gynecologic Obstetrics

Table 2. Comparison of radiomic features according to the tumor budding status.

	Total (n=76)	Intratumor budding			Peritumoral budding		
Valuables		Yes (n=47)	No (n=29)	p	Yes (n=62)	No (n=14)	p
Conventional metabolic parameters							
SUVmax							
Mean ± SD	12.30 ± 7.84	12.73 ± 6.48	11.60 ± 9.75	0.0406	12.11 ± 7.69	13.11 ± 8.76	0.8828
Median (range)	10.64 (3.28-48.94)	11.35 (5.25-39.79)	8.37 (3.28-48.94)		10.50 (4.13-48.94)	13.34 (3.28-35.52	
MTV							
Mean ± SD	20.64 ± 29.09	23.18 ± 34.60	16.52 ± 16.45	0.2548	20.78 ± 30.78	20.05 ± 20.82	0.8723
Median (range)	13.79 (2.15-220.0)	15.21 (2.44-220.00)	10.73 (2.15-76.79)		14.49 (2.15-220.00)	11.79 (6.51-76.79)	
TLG							
Mean ± SD	170.65 ± 478.22	219.30 ± 600.25	91.81 ± 101.10	0.0606	179.81 ± 526.27	130.08 ± 132.62	0.8407
Median (range)	78.75 (11.16-4118.4)	85.97 (15.76-4118.40)	57.09 (11.16-488.82)		78.74 (11.16-4118.40)	77.05 (19.25-488.82)	
Radiomic features							
GLCM							
Entropy GLCM							
Mean ± SD	7.68 ± 1.30	7.98 ± 1.10	7.21 ± 1.46	0.0111	7.70 ± 1.19	7.62 ± 1.76	0.8500
Median (range)	7.662 (4.89-10.22)	7.78 (5.85-10.22)	6.99 (4.89-9.88)		7.57 (4.98-10.22)	8.10 (4.89-9.88)	
NGLDM							
Coarseness							
Mean ± SD	0.0204 ± 0.0157	0.0170 ± 0.0128	0.0258 ± 0.0186	0.0497	0.0194 ± 0.0138	0.0249 ± 0.0225	0.7276
Median (range)	0.0140 (0.0002–0.0757)	0.0129 (0.0002-0.0514)	0.0239 (0.0025-0.0757)		0.0147 (0.0002-0.0560)	0.0125 (0.0054-0.0757)	

GLRLM							
Low Gray-level Run Emphasis	0.0073 ± 0.0040	0.0065 ± 0.0034	0.0087 ± 0.0044	0.0189	0.0068 ± 0.0034	0.0096 ± 0.0054	0.0939
Mean ± SD	0.0071	0.0057	0.0081		0.0062	0.0081	
Median (range)	(0.0013-0.0213)	(0.0013-0.0160)	(0.0020-20.0213)		(0.0013-0.0160)	(0.0020-0.0213)	
				0.0101			0.1266
Long-Run Low Gray-level Emphasis	0.0098 ± 0.0064	0.0085 ± 0.0056	0.0120 ± 0.0071		0.0090 ± 0.0054	0.0134 ± 0.0093	
Mean ± SD	0.0087	0.0069	0.0099		0.0084	0.0101	
Median (range)	(0.0014-0.0322)	(0.0014-0.0299)	(0.0022-0.0322)		(0.0014-0.0299)	(0.0022-0.0322)	

Continue

	Total (n=76)	Intratumor budding			Peritumoral budding		
Valuables		Yes (n=47)	No (n=29)	p	Yes (n=62)	No (n=14)	p
GLZLM							
Low Gray-level Zone Emphasis	0.0079 ± 0.0051	0.0069 ± 0.0045	0.0096 ± 0.0061	0.0137	0.0074 ± 0.0040	0.0104 ± 0.0081	0.2547
Mean ± SD							
Median (range)	0.0071 (0.0014-0.0327)	0.0060 (0.0014-0.0206)	0.0085 (0.0021-0.0327)		0.0070 (0.0014-0.0206)	0.0079 (0.0021-0.0327)	
Short-Zone Low Gray-level Emphasis	0.0045 ± 0.0026	0.0039 ± 0.0019	0.0054 ± 0.0033	0.0154	0.0042 ± 0.0020	0.0058 ± 0.0043	0.2177
Mean ± SD							
Median (range)	0.0039 (0.0008-0.0183)	0.0036 (0.0011-0.0100)	0.0047 (0.0084-0.0183)	0.0056	0.0038 (0.0008-0.0100)	0.0043 (0.0016-0.0183)	0.2492
Zone Length Non-Uniformity Zone	12.95 ± 11.89	15.47 ± 13.76	8.88 ± 6.28		13.53 ± 12.55	10.42 ± 8.22	
Mean ± SD	9.63 (1.88-80.85)	11.86 (3.40-80.85)	7.55 (1.88-32.24)		9.63 (1.88-80.85)	8.58 (2.77-32.24)	
Median (range)							
Shape and Size							
Sphericity	5208.48 ± 4024.88	5676.9 ± 4507.4	3963.1 ± 2723.4	0.0065	5238.6 ± 4203.5	5075.1 ± 3244.7	0.9040
Mean ± SD							
Median (range)	4249.8 (714.7-26258.1)	4894.7 (1227.2-26258.8)	3319.1 (714.7-11649.2)		4362.1 (1122.0-26258.8)	4005.5 (714.7-11649.2)	
Compacity				0.0108			0.4859
Mean ± SD	4.44 ± 1.32	4.75 ± 1.34	3.95 ± 1.16		4.42 ± 1.34	4.52 ± 1.29	
Median (range)	4.27 (2.27-8.88)	4.58 (2.76-8.88)	3.77 (2.27-6.28)		4.23 (2.39-8.88)	4.35 (2.27-6.28)	
Histogram							

Kurtosis							
Mean ± SD	3.00 ± 0.94	2.81 ± 0.68	3.30 ± 1.21	0.0267	2.94 ± 0.80	3.25 ± 1.42	0.7682
Median (range)	2.72 (1.76-7.47)	2.63 (1.76-5.05)	2.84 (2.12-7.47)		2.72 (1.76-5.96)	2.69 (2.15-7.47)	
$Entropy_{Hist}$				0.0130			0.9706
Mean ± SD	4.33 ± 0.76	4.50 ± 0.63	4.06 ± 0.88		4.33 ± 0.69	4.34 ± 1.05	
Median (range)	4.40 (2.68 – 5.74)	4.50 (3.18-5.74)	4.01 (2.68-5.49)	0.0200	4.36 (2.68-5.74)	4.77 (2.71-5.49)	0.7579
$Energy_{Hist}$							
Mean ± SD	0.0685 ± 0.0403	0.0591 ± 0.0320	0.0836 ± 0.0478		0.0670 ± 0.0372	0.0749 ± 0.0534	
Median (range)	0.0576 (0.0212-0.1820)	0.0518 (0.0212-0.1816)	0.0722 (0.0244-0.1820)		0.0603 (0.0212-0.1820)	0.0474 (0.0244-0.1685)	

GLCM = gray-level co-occurrence matrix; GLRLM = gray-level run length matrix; GLZLM = gray-level zone-length matrix; MTV = metabolic tumor volume; NGLDM = neighborhood gray-level different matrix; SUVmax= maximum standardized uptake; TLG= total lesion glycolysis.

Table 3. Multiple logistic regression analysis for the evaluation of the correlation between radiomic features and intratumor budding status.

	Univariate analysis			Multivariate analysis		
Variables	Odds ratio	95% CI	p	Odds ratio	95% CI	p
Conventional metabolic parameters						
SUVmax (> 8.858)	3.3393	1.2685-8.7908	0.0146	2.4973	0.8933-6.9810	0.0810
MTV (cm3, > 16.3)	2.5385	0.9092-7.0869	0.0753			
TLG (> 32.0247)	4.4211	1.3282-14.7159	0.0154			
Radiomic features						
GLCM						
EntropyGLCM (> 7.1782)	5.3554	1.9520-14.6928	0.0011	0.6139	0.0708-5.3208	0.6579
NGLDM						
Coarseness (≤ 0.0254)	3.9407	1.4085-11.0251	0.0090	1.0604	0.2057-5.4660	0.9441
GLRLM						
Low Gray-level Run Emphasis (≤ 0.0081)	3.4533	1.2588-9.4739	0.0161			
Long-Run Low Gray-level Emphasis (≤ 0.0094)	3.3393	1.2685-8.7908	0.0146	1.6936	0.4822-5.9481	0.4111
GLZLM						
Low Gray-level Zone Emphasis (≤ 0.0074)	4.0533	1.5196-10.8155	0.0052			
Short-Zone Low Gray-level Emphasis (≤ 0.005)	3.9407	1.4085-11.0251	0.0090			
Zone Length Non-Uniformity Zone (> 14.1652)	9.1607	1.9444-43.1600	0.0051	5.3971	0.9464-30.7790	0.0577
Shape and Size						
Sphericity (> 4160.0834)	6.0893	2.1463-17.2763	0.0007			
Compacity (> 3.4057)	8.7344	2.4798-30.7648	0.0007	5.0047	1.1636-21.5253	0.0305
Histogram						
Kurtosis (≤ 3.1264)	3.9609	1.3783-11.3826	0.0106			

$Entropy_{Hist}$ (> 4.0608)	5.9815	2.1219-16.8615	0.0007	2.9011	0.4526-18.5937	0.2611
$Energy_{Hist}$ (≤ 0.0688)	5.9815	2.1219-16.8615	0.0007			

CI= confidence interval GLCM= gray-level co-occurrence matrix; GLRLM= gray-level run length matrix; GLZLM= gray-level zone-length matrix; MTV= metabolic tumor volume; NGLDM= neighborhood gray-level different matrix; SUVmax= maximum standardized uptake; TLG= total lesion glycolysis.

Figures

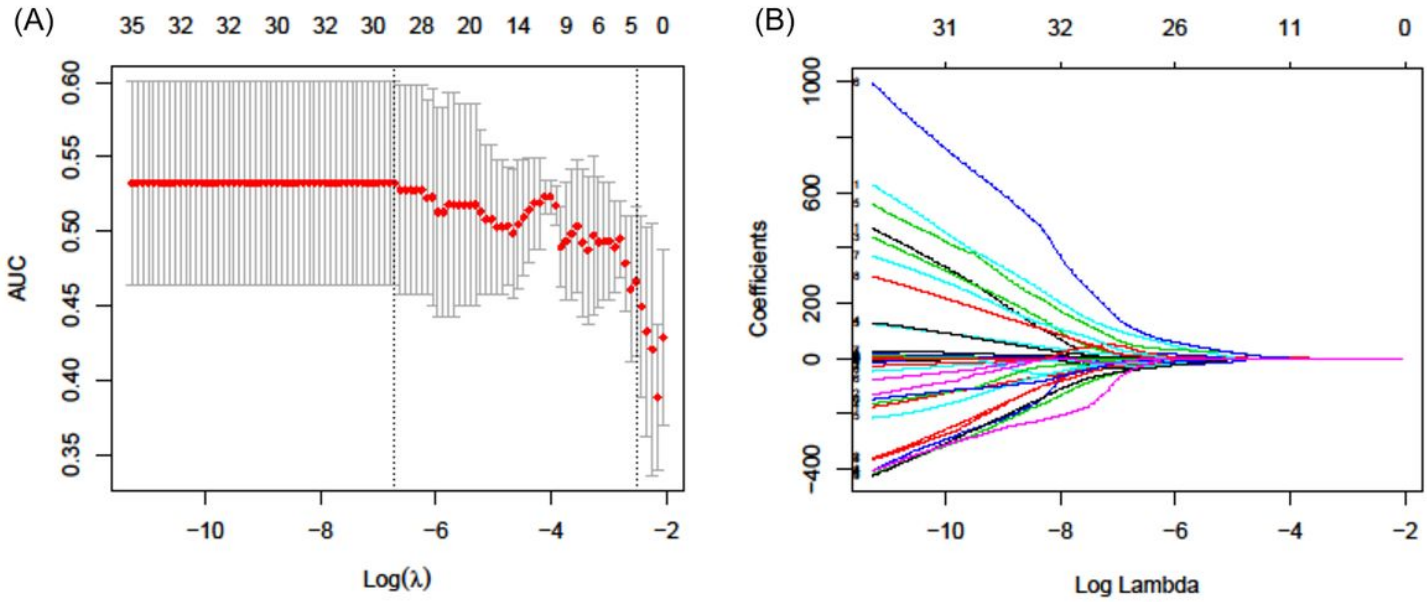

Figure 1

18F-FDG PET/CT radiomic feature selection was performed by the least absolute shrinkage and selection operator (LASSO) regularization method. (A) Area under the curve (AUC) was drawn versus log (λ) by the 5-fold cross-validation. The vertical dotted line defines the optimal λ value. Optimal λ of 0.0012, with log (λ) of -6.7061 was selected. (B) Lasso coefficient profiles of the 48 potential PET features which were selected by t-test. As a result, twenty seven features were selected with the optimal λ.

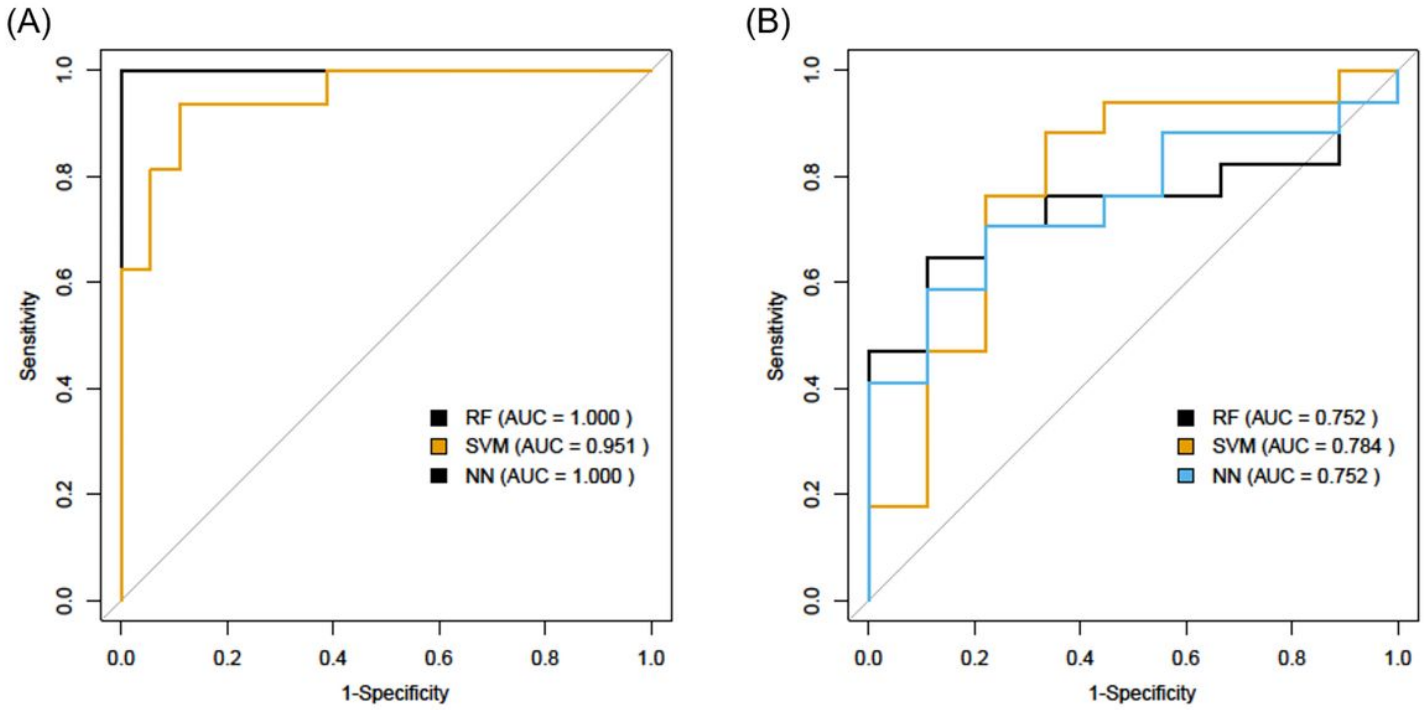

Figure 2

Receiver-operating characteristic (ROC) curves of the prediction models constructed by the random forest (RF), support vector machine (SVM), neural network (NN) algorithms using metabolic and radiomic features in the training dataset (A) and test dataset (B).

Supplementary Files

This is a list of supplementary files associated with this preprint. Click to download.

- SupplementaryTable1.docx